American Mineralogist, Volume 73, pages 677–691, 1988

TEM and X-ray study of orthopyroxene megacrysts: Microstructures and crystal chemistry

David R. Veblen
Department of Earth and Planetary Sciences, The Johns Hopkins University, Baltimore, Maryland 21218, U.S.A.
David L. Bish
Earth and Space Sciences Division, Mail Stop D469, Los Alamos National Laboratory, Los Alamos, New Mexico 87545, U.S.A.

Abstract

Single-crystal X-ray diffraction and light microscopy indicate that orthopyroxenes with pronounced (100) parting contain lamellae of amphibole and/or oxides. Detailed transmission electron-microscopy (TEM) and analytical electron-microscopy (AEM) studies of an orthopyroxene megacryst from an anorthosite demonstrate that this pyroxene is a complex mixture of several different types of lamellae, which have been characterized by electron diffraction, TEM imaging, and AEM analysis. The lamellae include host orthopyroxene, magnetite, hercynite, ilmenite, calcic plagioclase, augite, clinoamphibole, complex hybrid lamellae containing both clinopyroxene and clinoamphibole, and other types of hybrid lamellae involving both silicates and oxides.

Although optically the most obvious lamellae in this orthopyroxene megacryst are plagioclase and oxides, micrometer-sized to submicroscopic amphibole lamellae are by far the most abundant. Such amphibole lamellae are difficult to observe with standard petrographic techniques and may have been overlooked in previous studies of orthopyroxene megacrysts. Microstructures in the amphibole and in the hybrid pyroxene-amphibole lamellae indicate that amphibole formed by replacement of (100) exsolution lamellae of clinopyroxene. The presence of abundant amphibole suggests that this orthopyroxene megacryst experienced substantial hydrothermal alteration.

Introduction

Orthopyroxene megacrysts commonly occur in anorthosite massifs. They can grow up to 0.5 m in length and typically exhibit a pronounced parting parallel to (100). Although these orthopyroxene megacrysts generally are insignificant volumetrically, they have received attention in the recent petrologic literature, since they may place constraints on the evolution of anorthositic rocks (Emslie, 1975; Morse, 1975, 1979; Bohlen and Essene, 1978; Dymek and Gromet, 1984).

The Type I orthopyroxene megacrysts of Emslie (1975) have relatively aluminous bulk compositions and are reported to contain (100) lamellae of plagioclase, one or two oxides, and clinopyroxene. In the present study combining single-crystal X-ray diffraction, transmission electron microscopy (TEM), and light optical petrography, it is shown that (100) lamellae of amphibole also can be an important component of orthopyroxene megacrysts. In addition, analytical and imaging TEM experiments on a megacryst from Labrador show that these pyroxenes can be more complex than previously recognized. This megacryst contains at least nine distinct types of (100) lamellae, many of them smaller than the resolution of the light microscope: host orthopyroxene, chromian magnetite, hercynite, ilmenite, calcic plagioclase, clinopyroxene, clinoamphibole, microstructurally complex hybrid lamellae containing intimately intergrown clinopyroxene and clinoamphibole, and hybrid silicate-oxide lamellae.

The present paper describes the X-ray diffraction results, the chemical compositions of lamellae as determined by analytical electron microscopy (AEM), the intergrowth textures as ascertained by electron and light optical methods, the crystallographic relationships among the intergrown minerals, and the genetic implications of these observations. One obvious conclusion of this work is that these orthopyroxene megacrysts are chemically and microstructurally far more complex than the pyroxenes from basalts and gabbros that have been studied so extensively with transmission electron microscopy (for reviews see Buseck et al., 1980; Veblen, 1985). In addition, it is clear that they can be even more complex than previously thought from studies utilizing more standard petrographic techniques. In a subsequent paper, we will describe the detailed structures of grain boundaries in this intergrowth, as determined experimentally with high-resolution TEM and computer simulation of HRTEM images (Veblen and Bish, in prep.).

0003–004X/88/0708–0677$02.00

TABLE 1. Unit-cell parameters and structural formula of orthopyroxene 1507

$a = 1.825$ nm*	Space group = *Pbca*
$b = 0.883$ nm*	
$c = 0.519$ nm*	
$(Mg_{1.43}Fe_{0.47}Ca_{0.01}Al_{0.09})_{\Sigma 2.00}[Si_{1.93}Al_{0.07}]_{\Sigma 2.00}O_6$**	

* X-ray precession method.
** Electron-microprobe analysis; all Fe calculated as Fe^{2+}.

EXPERIMENTAL TECHNIQUES AND SPECIMEN DESCRIPTION

The primary specimen employed in this study is number 1507 from the mineral collection of Harvard University. Its locality is given as Labrador, and it is similar texturally and chemically to megacrysts described from the Nain anorthosite complex (see, for example, Morse, 1975). The pyroxene is dark brown and exhibits an excellent parting on (100). In addition, three other orthopyroxenes possessing excellent (100) partings were examined with X-ray diffraction, electron microscopy, and/or optical petrography: (1) an enstatite from an enstatite-serpentine rock from West-town, Chester County, Pennsylvania, Harvard Dana Collection number 103108; (2) an orthopyroxene megacryst from the Gore Mountain Gneiss, New York, collected by D.L.B.; and (3) a bronzite from Bamble, Norway, as previously described by Iijima and Buseck (1975).

X-ray diffraction studies were carried out with the precession method, utilizing Mo$K\alpha$ radiation. Electron-microprobe analysis was performed with an ARL-EMX probe using silicate standards. Unit-cell parameters and the structural formula of orthopyroxene 1507 as determined by electron-microprobe analysis are given in Table 1.

Specimens for TEM experiments were prepared by ion milling of petrographic thin sections cut parallel to (001), followed by C coating. Electron microscopy was performed with a Philips 420 transmission microscope operated at 120 kV and employing both an ST objective lens (spherical aberration coefficient $C_s = 1.2$, chromatic aberration coefficient $C_c = 1.2$) and a T objective lens ($C_s = 2.0$, $C_c = 2.0$). For HRTEM imaging, the objective aperture diameter either was matched to the point resolution of the microscope (0.30 nm for the ST lens and 0.34 nm for the T), or a smaller aperture was used to exclude irrelevant high-frequency information from the images.

X-ray spectra were collected with an EDAX SiLi detector and processed with a Princeton Gamma-Tech model 4000 analyzer, as described in detail by Livi and Veblen (1987). Background was subtracted using the TWIST algorithm of Aden and Buseck (1979), and characteristic peak intensities were obtained by a FRAMEC-type Gaussian decomposition (Myklebust et al., 1978). Elemental ratios were determined by the ratio method (Cliff and Lorimer, 1975), employing empirically determined $k_{X\text{-}Si}$ values for most elements and calculated values constrained by the empirical k values for Ti, Cr, and Ni. Oxides were analyzed using $k_{X\text{-}Fe}$ values obtained as the ratios of the pertinent $k_{X\text{-}Si}$ values.

X-RAY DIFFRACTION RESULTS

Orthopyroxene 1507 was found to produce diffractions on precession photographs not only from orthopyroxene, but also from clinoamphibole, augite, and at least two oxides oriented topotactically with respect to the pyroxene host. The pyroxene and amphibole share the b and c axes, and the amphibole a axes assume both of the two possible twin-related orientations in all specimens. Orthopyroxene unit-cell parameters measured from precession photographs are given in Table 1. Systematic absences are consistent with space group *Pbca* for the orthopyroxene and $I2/m$ for the clinoamphibole. The Gore Mountain specimen contains (100) lamellae of clinoamphibole; the West-town material produces diffractions consistent with (100) lamellae of an oxide; and the Bamble sample contains (100) lamellae of clinoamphibole, talc, and an oxide.

These results suggest that (100) lamellae of clinoamphibole and an oxide may be common constituents of orthopyroxenes that exhibit good (100) parting; the possible relationship between (100) lamellae and the parting will be discussed further in a subsequent paper (Veblen and Bish, in prep.). The results on specimen 1507 also show that amphibole can be a volumetrically significant component of Type I orthopyroxene megacrysts from anorthosites. It is possible that amphibole has been overlooked in previous studies because much of it occurs as lamellae with widths below the resolution of the light microscope. However, with hindsight based on the X-ray study, numerous amphibole lamellae in the micrometer size range are visible with the petrographic microscope in (001) thin sections of specimen 1507, suggesting that amphibole may have been identified as clinopyroxene in past studies and hence overlooked.

The precession photographs from the pyroxene 1507 show no indication of plagioclase, even though electron and light microscopy demonstrate that plagioclase lamellae are abundant. The absence of recognizable diffractions from feldspar presumably results from the irrational orientation of the plagioclase with respect to the orthopyroxene host.

ELECTRON-MICROSCOPY RESULTS

As noted in the Introduction, at least nine distinct types of (100) lamellae were recognized in the megacryst specimen 1507 chosen for electron-microscopy studies. Identification of the various phases was based on electron-diffraction patterns and AEM analyses, and the locations and local orientation variations of phase boundaries were determined from HRTEM and conventional TEM images.

TABLE 2. Orientations of (100) lamellae, periodicities shared with orthopyroxene, and fractional misfit with host lattice

Lamellae	Orientation with opx	Spacing shared (nm; from SAED)	Fractional misfit
Clinoamphibole	$a_{opx} \| a^*_{am}$	$d_{100} = 0.948$	
	$b_{opx} \| b_{am}$	$b = 1.801$	0.020
	$c_{opx} \| c_{am}$	$c = 0.531$†	0.023
Clinopyroxene	$a_{opx} \| a^*_{cpx}$	$d_{100} = 0.948$	
	$b_{opx} \| b_{cpx}$	$b = 0.886$	0.003
	$c_{opx} \| c_{cpx}$	Not measured	
Chromian magnetite	$a_{opx} \| [111]_{mt}$	$d_{111} = 0.486$	
	$b_{opx} \| [110]_{mt}$	$3 \times d_{220} = 0.891$	0.009
	$c_{opx} \| [\bar{1}\bar{1}2]_{mt}$	$3 \times d_{224} = 0.514$‡	0.010
Hercynite	$a_{opx} \| [111]_{hc}$	$d_{111} = 0.472$	
	$b_{opx} \| [110]_{hc}$	$3 \times d_{220} = 0.864$	0.022
	$c_{opx} \| [\bar{1}\bar{1}2]_{hc}$	$3 \times d_{224} = 0.498$‡	0.040
Ilmenite (hexagonal cell setting)	$a_{opx} \| [001]_{il}$	$\frac{1}{3} \times d_{001} = 0.469$	
	$b_{opx} \| [100]_{il}$	$6 \times d_{300} = 0.883$	0.000
	$c_{opx} \| [\bar{1}20]_{il}$	$2 \times d_{120} = 0.509$‡	0.019
Plagioclase	variable	variable	variable

† c of amphibole measured from X-ray precession films.
‡ These parameters calculated from SAED-determined unit-cell parameters, but not measured directly on SAED films.

Orientation relationships between the structures of host orthopyroxene and included minerals were determined from electron-diffraction patterns containing diffraction spots from both the orthopyroxene host and a lamella. Unit-cell parameters of the lamellae were also determined from these patterns, utilizing orthopyroxene as an internal standard. The use of pyroxene as a diffraction standard assumes that local variations in unit-cell parameters due to chemical inhomogeneities are minor. It has been noted in some megacryst occurrences that the orthopyroxene host is partially depleted in Al near the plagioclase lamellae, but that the pyroxene is relatively homogeneous with respect to other major elements (Dymek and Gromet, 1984; Emslie, 1975). However, the observed variations in Al should produce unit-cell parameter errors less than 0.1% (LeFèvre, 1969; Deer et al., 1978, p. 26), less than other measurement errors. The sharpness of orthopyroxene diffractions on precession photographs from specimen 1507 also shows that there is little variation in orthopyroxene unit-cell parameters, again suggesting that use of the host diffractions as an internal standard is valid. With the use of an internal standard, unit-cell parameters measured from electron-diffraction patterns should be accurate to within 1% or less.

The orientation relationships between orthopyroxene and the other lamellae are summarized in Table 2, and chemical compositions derived from AEM analyses are given in Table 3. The orthopyroxene AEM analysis compares well with the electron-microprobe analysis reported in Table 1. Unit-cell translations of lamellae parallel to the orthopyroxene b axis were measured from electron-diffraction patterns, whereas parameters parallel to c were calculated from lattice parameters and the observed orientation relationships (see below for details on different lamellae). The structural formulae given in Table 3 were derived by adjusting the Fe^{2+}/Fe^{3+} ratio to achieve charge balance. Different types of lamellae found in the orthopyroxene host are discussed individually below.

Chromian magnetite

Titanian magnetite has been reported in orthopyroxene megacrysts from anorthosites as granules and (100) lamellae; rare (010) lamellae of magnetite also have been identified tentatively (Morse, 1975). Unspecified Fe-rich opaque oxides have been noted by Emslie (1975) in a number of occurrences. In the present study (specimen 1507), Fe-rich spinel lamellae have been identified con-

TABLE 3. Structural formulae from AEM analyses

	Orthopyroxene (12)	Clinoamphibole (14)	Clinopyroxene (15)		Plagioclase (7)		Hercynite (10)	Magnetite (4)	Ilmenite (3)
Si	1.93(2)	6.51(10)	1.82(5)	Si	2.08(3)	Fe^{2+}**	0.45(5)	1.02(13)	0.76(16)
Al	0.07(3)	1.49(13)	0.18(4)	Al	1.83(4)	Fe^{3+}	0.24(6)	1.39(14)	0.38(31)
Σ_{tet}	2.00	8.00	2.00	Fe^{3+}	0.09(5)	Mg	0.52(5)	0.00	0.00
Ca	0.01(1)	1.84(12)	0.63(16)	Σ_{tet}	4.00	Al	1.58(10)	0.00	0.00
Mg	1.49(3)	3.84(13)	0.99(9)	Na	0.05(2)	Ti	0.00	0.09(10)	0.81(15)
Fe*	0.45(1)	0.82(8)	0.25(8)	Ca	0.97(5)	Cr	0.18(5)	0.44(13)	0.01(1)
Al	0.04	0.36	0.05	Ni	0.01(1)	Mn	0.01(1)	0.02(1)	0.02(1)
Ti	0.00	0.12(2)	0.06(1)	Σ_{alk}	1.03	Ni	0.02(1)	0.04(2)	0.02(1)
Cr	0.01(1)	0.04(1)	0.01(1)			Σ_{cat}	3.00	3.00	2.00
Mn	0.01(1)	0.00	0.00						
Ni	0.01(1)	0.04(1)	0.00						
Σ_{oct}	2.02	7.06	1.99						
Na_A		0.67(9)							

Note: In column headings, numbers in parentheses are the number of analysis points for each mineral. Other numbers in parentheses are 1σ for the population of analyses, e.g., (2) indicates $1\sigma = 0.02$. For Al, σ is for total Al in the analysis. For the oxides, σ for total Fe is considerably lower than those for the Fe^{2+} and Fe^{3+} values consistent with charge balance.
* All Fe calculated as Fe^{2+}.
** Fe^{2+}/Fe^{3+} ratios adjusted to yield ideal cation sum.

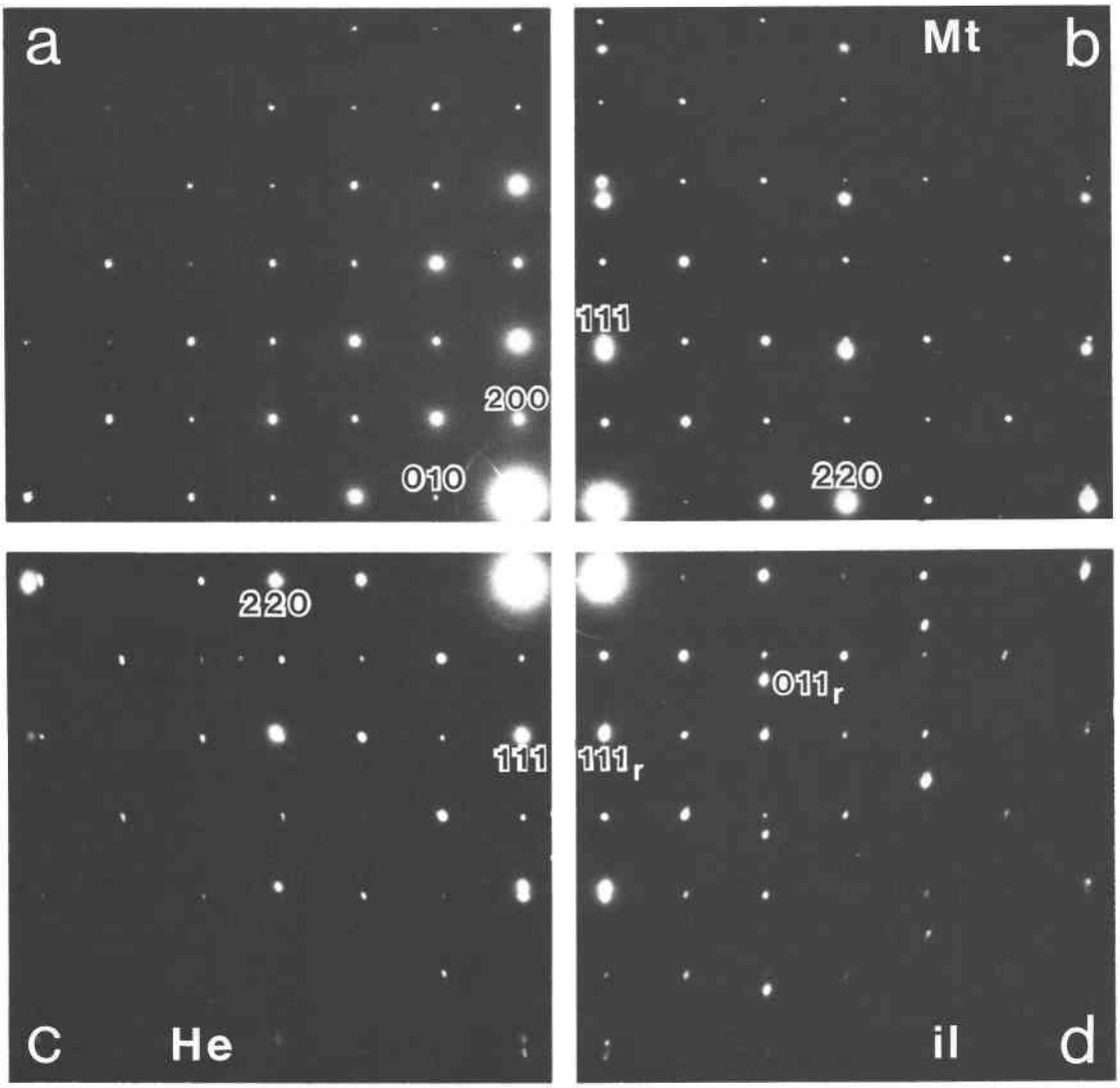

Fig. 1. Selected-area electron diffraction (SAED) patterns of oxides intergrown with orthopyroxene, taken parallel to the pyroxene c axis. (**a**) Pattern from pure orthopyroxene. (**b**) Orthopyroxene intergrown with magnetite, with the 111 and 220 magnetite diffractions labeled. (**c**) Orthopyroxene intergrown with hercynite, with the 111 and 220 hercynite diffractions indicated. (**d**) Orthopyroxene intergrown with ilmenite, with the 111 and 011 diffractions from ilmenite labeled (indexed on the rhombohedral cell setting).

clusively with a combination of electron-diffraction and AEM analyses. Unlike the oxides of previous reports, these magnetites are all Cr-rich (Table 3), with variable contents of chromite component up to approximately 0.6 Cr atoms per formula unit (four oxygens).

Figure 1a shows a selected-area electron-diffraction (SAED) pattern of host orthopyroxene, and Figure 1b shows a pattern with diffractions from both a chromian magnetite lamella and adjoining orthopyroxene host. This composite pattern shows the magnetite to be oriented as given in Table 2 and also shows that the match between the periodicities of the two lattices is very good parallel to b_{opx}. The calculated match between the pyroxene and magnetite parallel to c_{opx}, the other shared direction in the plane of the intergrowth, is also close, as shown in Table 2. In this orientation, the closest-packed (111) oxygen layers of magnetite are parallel to (100) of orthopyroxene; the oxygen layers parallel to this plane in pyroxene are in positions close to those of a closest-packed arrangement. A more detailed discussion of the intergrowth orientations and misfits is given below.

A HRTEM image of a grain boundary between orthopyroxene and magnetite is shown in Figure 2a. The interface is sharp, planar, and parallel to (100) of the pyroxene. Figure 2b shows the rounded termination of a magnetite lamella in orthopyroxene. Similar interfaces and terminations are also typical of the other types of oxide lamellae in this specimen.

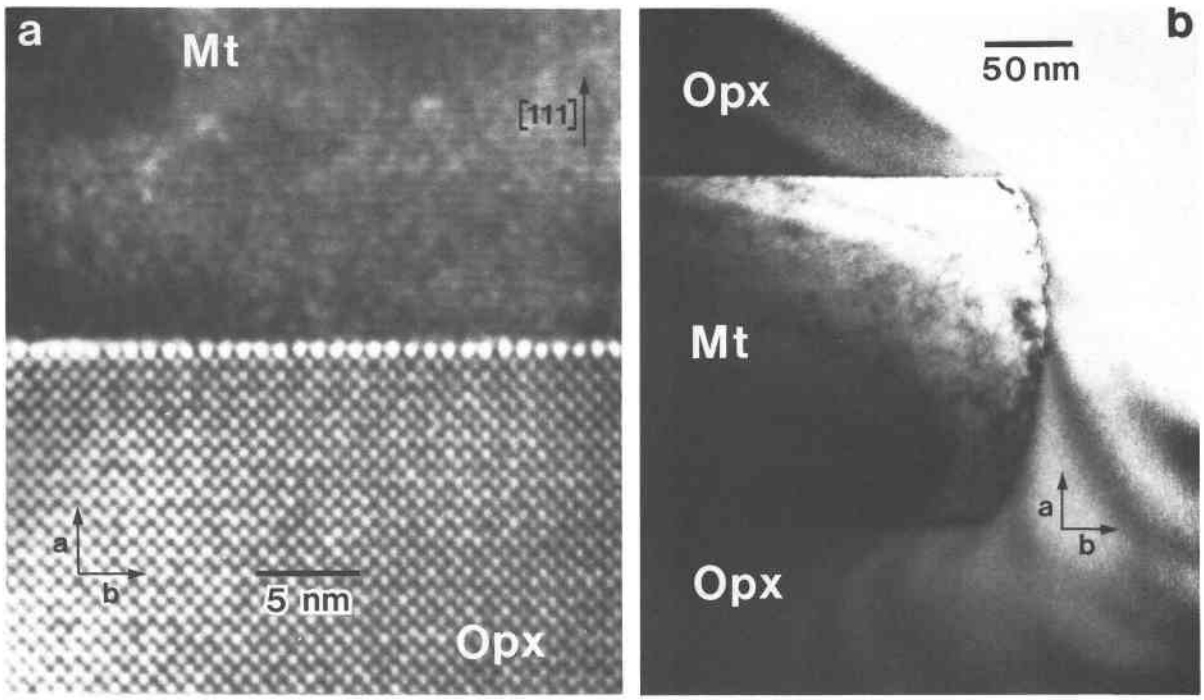

Fig. 2. (100) magnetite (Mt) lamellae in orthopyroxene (Opx). (**a**) HRTEM image of a typical pyroxene-magnetite interface, which is sharp and rigorously parallel to (100) of the pyroxene and (111) of the oxide. (**b**) Low-magnification view of the rounded termination of a magnetite lamella in orthopyroxene.

Hercynite

Hercynite has not been reported previously in orthopyroxene megacrysts from anorthosites. However, hercynite is the most abundant lamellar oxide in specimen 1507 and clearly is an important sink for Al during subsolidus reaction of the pyroxene. A SAED pattern from a hercynite lamella and surrounding orthopyroxene is shown in Figure 1c, and average composition, orientation, and degree of fit with the host pyroxene lattice are given in Tables 2 and 3. The hercynite contains substantial amounts of Mg and Cr, in addition to Fe and Al. In most respects the hercynite intergrowths with pyroxene are similar to those of magnetite. However, due to the smaller unit cell of hercynite, the misfit with pyroxene parallel to b_{opx} has the opposite sense compared to that of magnetite, as can be seen by comparing the electron-diffraction patterns in Figures 1b and 1c.

Ilmenite

Dymek and Gromet (1984) reported hemoilmenite as the lamellar oxide mineral in orthopyroxene megacrysts from the St. Urbain anorthosite massif in Quebec, and Morse (1975) reported ilmenite as an occasional constituent of megacrysts. Emslie (1975) reported hematite in several orthopyroxene megacrysts, on the basis of optical observations.

Average composition, orientation, and misfit of the ilmenite lamellae with the orthopyroxene host are given in Tables 2 and 3, and a SAED pattern is shown in Figure 1d. Just as the magnetite and hercynite lamellae share their closest-packed oxygen layers with (100) of the pyroxene, the closest-packed (001) layers of ilmenite are parallel to $(100)_{opx}$.

Clinopyroxene

Though reported as common constituents of orthopyroxene megacrysts from anorthosites, clinopyroxene lamellae in specimen 1507 are rather rare (less abundant than magnetite, hercynite, ilmenite, amphibole, and plagioclase). All clinopyroxene lamellae observed with the TEM are narrower than the resolution of the light microscope (typically from about 10 to 100 nm wide). Although it is clear that many reported clinopyroxene lamellae in orthopyroxene megacrysts from anorthosites are indeed pyroxene (e.g., those analyzed and given in Table 1 of Dymek and Gromet, 1984), it is possible that in some other cases clinoamphibole has been optically misidentified as clinopyroxene (an easy thing to do when one is dealing with micrometer-scale lamellae).

Clinopyroxene lamellae can be recognized easily in the TEM because they produce noticeably different contrast compared to host orthopyroxene, yet they produce *c*-axis HRTEM images with perodicities characteristic of pyroxene. Although all observed clinopyroxene lamellae were too narrow to isolate for SAED patterns, *c*-axis convergent-beam diffraction patterns (Fig. 3a) show that the h +

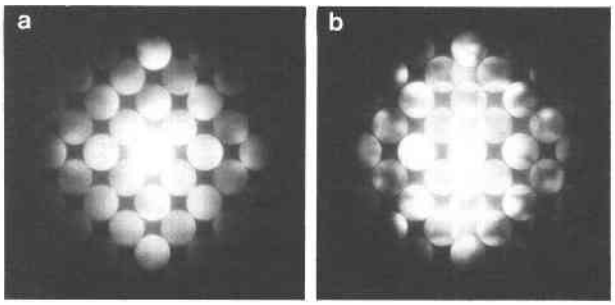

Fig. 3. Convergent-beam electron diffraction (CBED) patterns of (**a**) *C*-centered clinopyroxene. (**b**) Orthopyroxene. Extra diffractions in the orthopyroxene pattern differentiate it from clinopyroxene.

$k = 2n + 1$ diffractions are missing, as a result of *C*-centering (lattice-centering absences are preserved, even for dynamical electron diffraction). This convergent-beam pattern contrasts with that from host orthopyroxene (Fig. 3b), in which $h/2 + k = 2n + 1$ diffractions are observed in the positions of the clinopyroxene absences. The SAED patterns from both the orthopyroxene and clinopyroxene also show the systematic absences for the clinopyroxene *C*-centering and demonstrate that although there is misfit between the two pyroxenes in both d_{100} and d_{010}, it is less pronounced parallel to *b* (Table 2). Conventional TEM imaging experiments indicate that the (100) interfaces are semicoherent, consistent with the misfit observed in SAED patterns.

The AEM analyses indicate that the clinopyroxene is aluminous augite (Table 3). The very small size of the lamellae results in contamination of many of the analyses by the host orthopyroxene; this in turn causes wide variations in the Ca/(Mg + Fe) ratios and in the standard deviations for these elements reported in Table 3. The apparent Ca contents range from approximately 0.4 to 0.9 per formula unit based on six oxygens. Assuming that the highest Ca values correspond to the analyses that are the least contaminated by orthopyroxene, the composition is consistent with equilibration between host and lamellae below approximately 700 °C. This relatively low temperature is also consistent with the very low Ca contents of the orthopyroxene, which yield a two-pyroxene temperature in the neighborhood of 500 °C (Lindsley, 1983).

Clinoamphibole

By far the most abundant lamellae in specimen 1507 are clinoamphibole, consistent with the single-crystal X-ray diffraction results. Previous studies of amphiboles intergrown with pyroxenes include those by Smith (1977), Yamaguchi et al. (1978), Desnoyers (1975), Nakajima and Ribbe (1980), Isaacs et al. (1981), Veblen and Buseck (1981), and Mellini et al. (1983). AEM indicates that the amphibole is a pargasitic hornblende (Table 3; Leake, 1978), and composite SAED patterns from amphibole and host orthopyroxene show that the amphibole is *C*-centered (Fig. 4). The lamellae range in width from a few tens of nanometers to several micrometers, with the bulk of them falling in the optically unresolvable or barely resolvable range. Some of the lamellae (especially the narrower ones) exhibit a single amphibole orientation, but in many cases they are twinned either singly or multiply on (100). As is usual in pyriboles, most of the (100) twin planes are perfectly straight; in some cases, however, they are stepped, with sections parallel to (010) (Fig. 5).The interfaces between orthopyroxene and amphibole generally are roughly parallel to (100), but steps and local deviations from (100) orientations are not uncommon (Fig. 6a). Some amphibole lamellae are observed to terminate, change substantially in width, or have irregular shapes (Figs. 6b, 6c), although they are most commonly quite continuous in (100) and of roughly constant width. The grain-boundary structures between the amphibole and pyroxene are discussed in detail by Veblen and Bish (in prep.).

All of the clinoamphibole lamellae contain chain-width errors parallel to (010), although a few of the wider lamellae were observed to be nearly free of these defects. The chain widths of all these defects were single (pyroxene structure), triple (clinojimthompsonite structure), quadruple, or paired single (i.e., two adjacent single-chain slabs); since they have not been reported previously, a HRTEM image of a paired single-chain defect is shown in Figure 7. As discussed in detail by Veblen and Buseck (1981), when a pyroxene is replaced by nucleation and growth of amphibole, the amphibole domains growing from two adjacent nucleation events can grow together either with no mismatch or with a mismatch having an out-of-phase vector corresponding to chain-width defects containing single, triple, or quadruple chains (these domain boundaries were called polysomatic out-of-phase boundaries by Veblen and Buseck, 1981; see their Fig. 29). The displacement caused by a chain-width error consisting of two adjacent single chains is equivalent to that produced by a quadruple-chain error. The presence of these chain-width errors thus suggests an origin for the amphibole by reaction from primary clinopyroxene lamellae; the types of chain-width errors in this specimen are not consistent with an origin by alteration of the amphibole (see Veblen, 1981, and references therein).

If the amphibole lamellae arose by reaction from previously exsolved clinopyroxene, the number of single-chain errors, the number of triple-chain errors, and the sum of the numbers of quadruple-chain and paired single-chain errors should be equal (assuming random nucleation of amphibole in the pyroxene). The numbers of chain-width errors of different types observed in 22 amphibole lamellae using HRTEM images are as follows: 62 single, 52 triple, 5 quadruple, and 40 paired single. These observed numbers of the three different displacement vectors are all equal within two standard deviations (from counting statistics). There would be no reason to expect this equality if the chain-width errors arose as growth defects during direct exsolution of amphibole from the

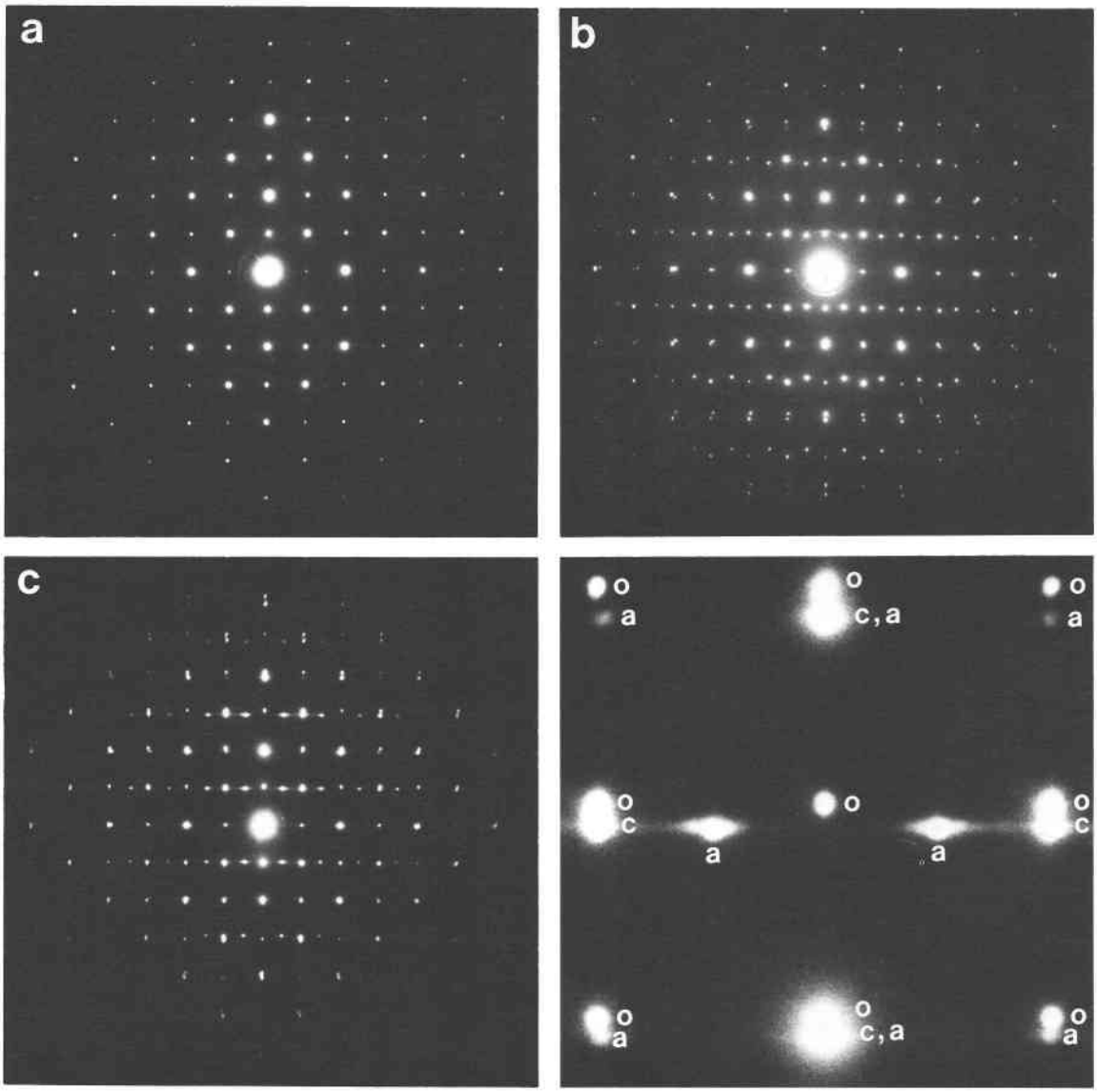

Fig. 4. SAED patterns taken parallel to the c axis of pyribole intergrowths; a^* is vertical and b^* is horizontal. (**a**) SAED pattern of pure orthopyroxene for reference. (**b**) Composite pattern from orthopyroxene host and clinoamphibole lamella. (**c**) Pattern from orthopyroxene and a hybrid lamella containing clinopyroxene and clinoamphibole. To the right is an enlargement of part of this pattern, with diffractions labeled. This shows streaking and elongation of the amphibole and clinopyroxene diffractions parallel to b^*, due to shape effects and structural disorder of the narrow lamellae (o = orthopyroxene, c = clinopyroxene, a = amphibole).

orthopyroxene. Thus, both the presence and numbers of different types of chain-width errors suggest that the (100) amphibole lamellae arose not by direct precipitation from the host orthopyroxene, but rather by the replacement of previously exsolved (100) clinopyroxene lamellae.

Assuming that the chain-width errors did, indeed, arise as out-of-phase boundaries between independently nucleated amphibole domains, their frequency ideally can be used to determine a nucleation density for amphibole in the clinopyroxene lamellae. However, the larger lamellae contain fewer chain-width errors than the small ones, suggesting that these defects have annealed out of the larger lamellae. Among the smaller lamellae (<0.2-μm width), the average spacing of chain-width errors is observed to be between 13 and 20 nm. Since one-fourth of the nuclei pairs grow together in phase (i.e., with no chain-width error) for random nucleation, the observed spacing suggests that amphibole nuclei formed approximately 10 to 15 nm apart in the [010] direction. Actual distances between nuclei could have been smaller, as a result of subsequent removal of chain-width errors during annealing.

Most of the chain-width errors in the clinoamphibole lamellae are perfectly parallel to (010) and are continuous

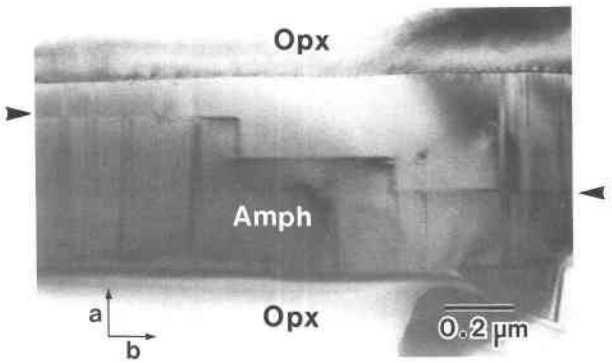

Fig. 5. A (100) amphibole lamella in orthopyroxene, showing a stepped twin plane running between the two arrows. Vertical features within the amphibole lamella are chain-width errors.

from one pyroxene-amphibole interface to the other. There are, however, exceptions to this general observation. For example, chain-width errors in some cases are observed to terminate within an amphibole lamella. Such a termination may represent a stage in the removal of the defect during annealing. In some cases, chain-width errors are observed to terminate at (100) twin planes or stacking faults in amphibole (Fig. 8).

There are also exceptions to the usual (010) orientation of chain-width errors. Figure 9a shows curved chain-width errors and an example of two such errors connected by a curved section of a displacive planar fault (as is usual when describing defects, "planar" here means two-dimensional, rather than strictly planar). An unusual curved chain-width error is shown intersecting another chain-width error in Figure 9b. High-resolution images show that both defects are single-chain lamellae and that when they combine, they form a quadruple-chain defect. Although such addition of two defects to form a different type of defect is not unusual, it has not been reported previously in pyriboles.

Hybrid clinopyroxene-clinoamphibole lamellae

The most unusual lamellae observed in specimen 1507 are two-phase, hybrid lamellae consisting of intimately intergrown clinopyroxene and clinoamphibole. Like the other lamellae in this specimen, these hybrid lamellae are parallel to (100), with the pyroxene and amphibole sections sharing (010), as shown in Figure 10. With these interface orientations, the clinopyroxene-orthopyroxene boundaries can be structurally continuous (no dangling bonds), as can the clinopyroxene-clinoamphibole interfaces. On the other hand, roughly half of the bonds in the orthopyroxene-clinoamphibole interfaces can be bonds typical of pyribole structures, while the other half are not satisfied normally (see Veblen and Bish, in prep., for details on the structure of these orthopyroxene-clinoamphibole boundaries). X-ray analyses show that the compositions of the pyroxene and amphibole are approximately the same as those in the pure clinopyroxene and pure amphibole lamellae, respectively. A SAED

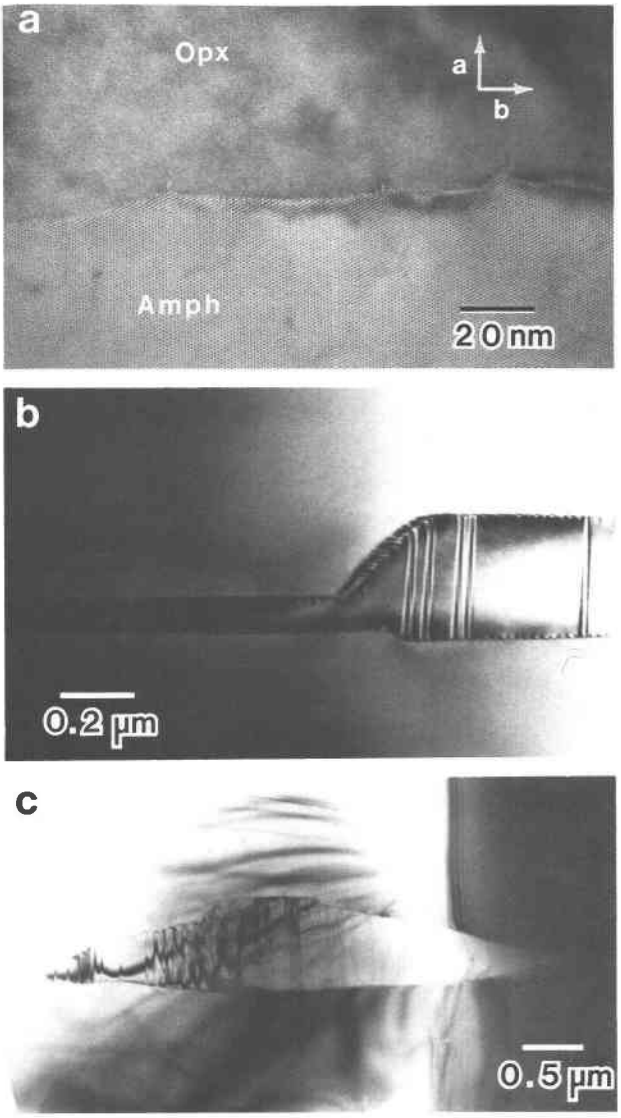

Fig. 6. Amphibole lamellae showing deviations from the usual (100) interface orientation with orthopyroxene. (**a**) An irregular interface. (**b**) An amphibole lamella exhibiting a pronounced change in width. (**c**) A lens-shaped amphibole lamella. Vertical features in the amphibole lamellae of a, b, and c are all chain-width errors in different contrast.

pattern of host orthopyroxene with a hybrid lamella is shown in Figure 4c, and an enlarged portion of the pattern is shown in Figure 4d with diffractions from the three structures labeled. The amphibole diffractions exhibit considerable diffuseness parallel to b^*, as a result of substantial chain-width disorder in the region from which this pattern was recorded.

The relatively high thermal stability limit of pargasitic hornblende (Gilbert et al., 1982) does not rule out the possibility that these hybrid pyroxene-amphibole lamellae arose by direct coprecipitation from the orthopyroxene host. However, such an origin seems unlikely on other grounds. Differences in the a, c, and β unit-cell

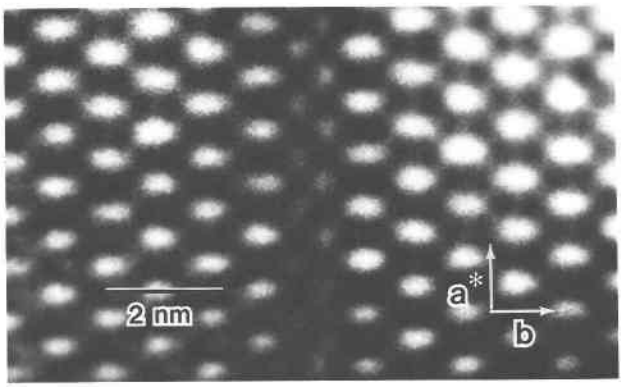

Fig. 7. HRTEM image of a chain-width error that is two single chains wide (i.e., it consists of two narrow slabs of pyroxene structure). Defects of this type occur commonly in the amphibole lamellae of pyroxene 1507.

parameters indicate that the (010) interface planes of the two clinopyriboles involve considerable strain, and separate (100) clinopyroxene and clinoamphibole lamellae should be energetically favored in a precipitation process. Furthermore, most of the amphibole sections of the hybrid lamellae contain an even number of amphibole chains in the *b* direction. It has been observed in a number of occurrences that the reaction of pyroxene to amphibole favors such even-width amphibole lamellae. Therefore, it seems most likely that the amphibole in the hybrid lamellae formed by partial replacement of initially pure (100) clinopyroxene lamellae. Thus, these unusual hybrid lamellae probably represent an intermediate stage of reaction between the pure clinopyroxene and pure amphibole lamellae that are observed in this specimen. The average spacing measured between amphibole segments in the hybrid lamellae is approximately 28 nm. Like the spacing between out-of-phase domains in the amphibole

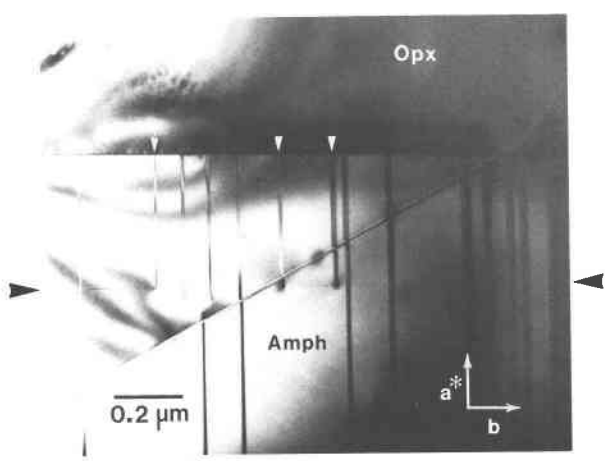

Fig. 8. Chain-width errors (white arrows) terminating at a (100) stacking fault (sharp line between black arrows) in an amphibole lamella. Other chain-width errors continue through the stacking fault. Sharp line slanting from upper right to lower left is from fracture of the specimen along cleavage.

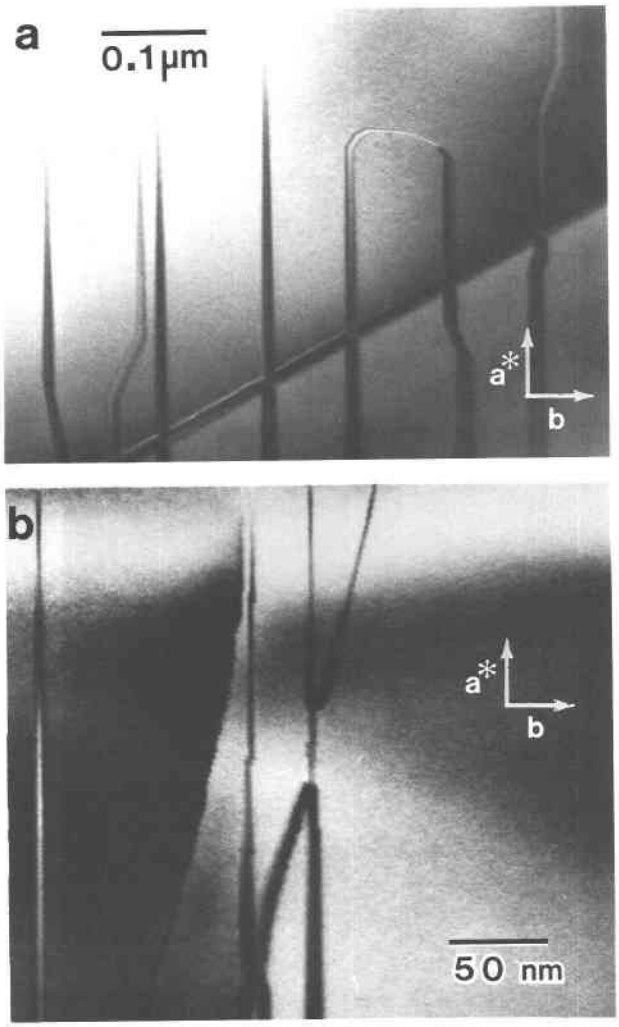

Fig. 9. Chain-width errors in orientations other than (010). (**a**) Curving of chain-width errors; two of these defects are connected by a region of displacive planar fault. (**b**) Two intersecting chain-width errors combine to form a short defect having their combined fault vector (see text). The feature across which contrast changes abruptly is a twin plane far from the usual (100) orientation.

lamellae, this is presumably a measure of the nucleation density of amphibole in clinopyroxene lamellae and is of the same order of magnitude as the former calculation of one nucleus every 10 to 15 nm.

Plagioclase

Although they are far less numerous than the amphibole lamellae, the plagioclase lamellae in specimen 1507 are the largest. As observed for other occurrences, the plagioclase is quite calcic (Table 3) and typically is twinned. No compositional zoning was detected with AEM analyses across submicrometer lamellae. Although the orthopyroxene-plagioclase interfaces are oriented parallel to the orthopyroxene (100), the orientation of the plagioclase with respect to the orthopyroxene crystallographic

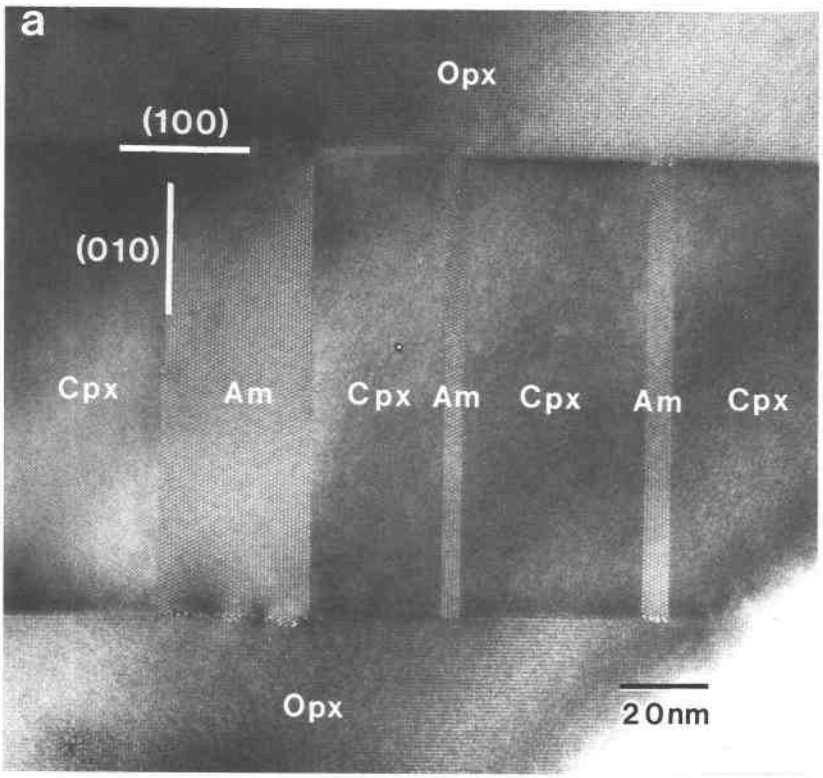
a
Opx
(100)
(010)
Cpx
Am
Cpx
Am
Cpx
Am
Cpx
Opx
20nm

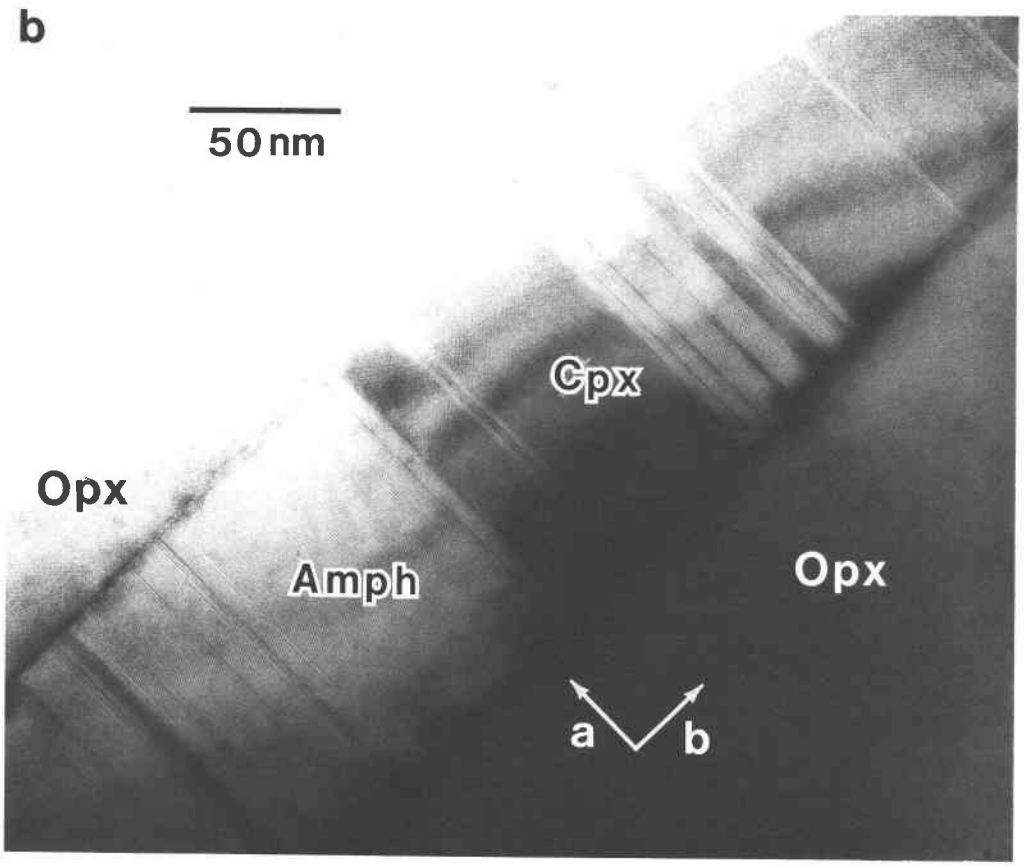
b
50nm
Cpx
Opx
Amph
Opx
a
b

axes is irrational and variable, as noted for other occurrences (Morse, 1975; Emslie, 1975; Dymek and Gromet, 1984).

Minor minerals

In addition to the lamellae of orthopyroxene, oxides, clinopyroxene, clinoamphibole, and plagioclase, two other minerals were observed as very minor constituents of specimen 1507. Small inclusions of chlorite were observed along one amphibole lamella; it is most likely a low-temperature alteration or weathering product and will not be considered further. Likewise, a small amount of a mineral that is probably (Mg,Ca,Fe) carbonate was observed in one area and will not be discussed further.

Combination lamellae

It has been noted in previous studies of orthopyroxene megacrysts from anorthosites that plagioclase lamellae commonly are discontinuous, containing segments of oxide (ilmenite or magnetite). This important observation of combination lamellae has been used to infer that the plagioclase and oxide formed concurrently by precipitation (exsolution) from the orthopyroxene host. The same phenomenon is observed in specimen 1507 with the TEM, as well as with the petrographic microscope (see below). In addition, several other, previously undescribed types of combination lamellae have been observed: (1) Plagioclase lamellae can contain segments not only of oxide, but also of amphibole. (2) Uncommonly, lamellae contain both clinopyroxene or amphibole and an oxide, intergrown on (100). (3) Although most lamellae are rather simple, there do exist regions of complex texture where several different minerals coexist in a small area. For example, one lamella was observed to contain plagioclase, amphibole, hercynite, ilmenite, and an unidentified mineral in a complicated intergrowth.

Light-microscopy results

Thin sections cut parallel to the host orthopyroxene (100), (010), and (001) planes were studied with both transmitted- and reflected-light microscopy. In many respects the observations from (010) and (001) sections are similar to those of Emslie (1975), Morse (1975, 1979), and Dymek and Gromet (1984), and photomicrographs similar to theirs are not reproduced here. Petrographic observations bearing on cleavage and parting mechanisms will be presented by Veblen and Bish (in preparation).

Host orthopyroxene

The orthopyroxene possesses the typical pinkish-brown pleochroism parallel to the b axis. In places, it does not go to perfect extinction in cross-polarized light, presumably as a result of the numerous included submicrometer lamellae of various sorts, but is otherwise optically normal.

Oxide lamellae

In (010) and (001) sections, hercynite appears as thin, olive-green, isotropic lamellae, and magnetite and ilmenite are opaque. The thicker lamellae of all three oxides (a few micrometers thick) commonly form segments of compound lamellae with plagioclase, although some of the hercynite lamellae are isolated. In (001) sections, the thinner opaque lamellae (<1 μm wide) appear to occur preferentially as compound lamellae with a mineral having extremely low contrast, presumably amphibole.

In (100) sections, it can be seen that the hercynite lamellae are plates of irregular shape and are not elongated preferentially parallel to a or c of the host (Fig. 11a); they range from approximately 20 to 50 μm in extent. Many of the hercynite lamellae possess a small marginal crystal of ilmenite (Fig. 11b), which presumably formed by late-stage exsolution from the hercynite or surrounding plagioclase. In this (100) orientation, magnetite appears as irregular, opaque plates on the order of 100 μm across, and ilmenite is light clove-brown to opaque, depending on thickness. Although some of the ilmenite lamellae are irregular in shape, most are elongated parallel to either c or b of the host orthopyroxene (Fig. 11c).

Pyribole lamellae

Amphibole is observed in (010) sections as thin lamellae up to 4 μm wide and having extinction angles of approximately 15–25° with respect to the c axis. The observed extinction is consistent with pargasitic hornblende and not augite. There are two sets of amphibole lamellae having different orientations related to each other by the mirror component of the orthopyroxene b-glide parallel to (100); some of the larger lamellae are twinned simply or multiply on (100). No indication of clinopyroxene was found, in keeping with the TEM observation that remnant augite lamellae are very narrow (in the range of tens of nanometers thick). In (001) sections, lamellae having extremely low contrast in reflected, plane-, and cross-polarized light are interpreted to be amphibole. In all cases, amphibole lamellae appeared to be perfectly planar, parallel to (100) of the host orthopyroxene, and up to several

←

Fig. 10. (**a**) An example of a hybrid (100) clinopyroxene-amphibole lamella in orthopyroxene. The clinopyroxene and clinoamphibole intergrow on (010). (**b**) Another hybrid lamella, showing that the amphibole and clinopyroxene lamellae can contain substantial chain-width disorder. This disorder leads to streaking of amphibole and clinopyroxene diffractions parallel to b^*, as shown in Fig. 4c.

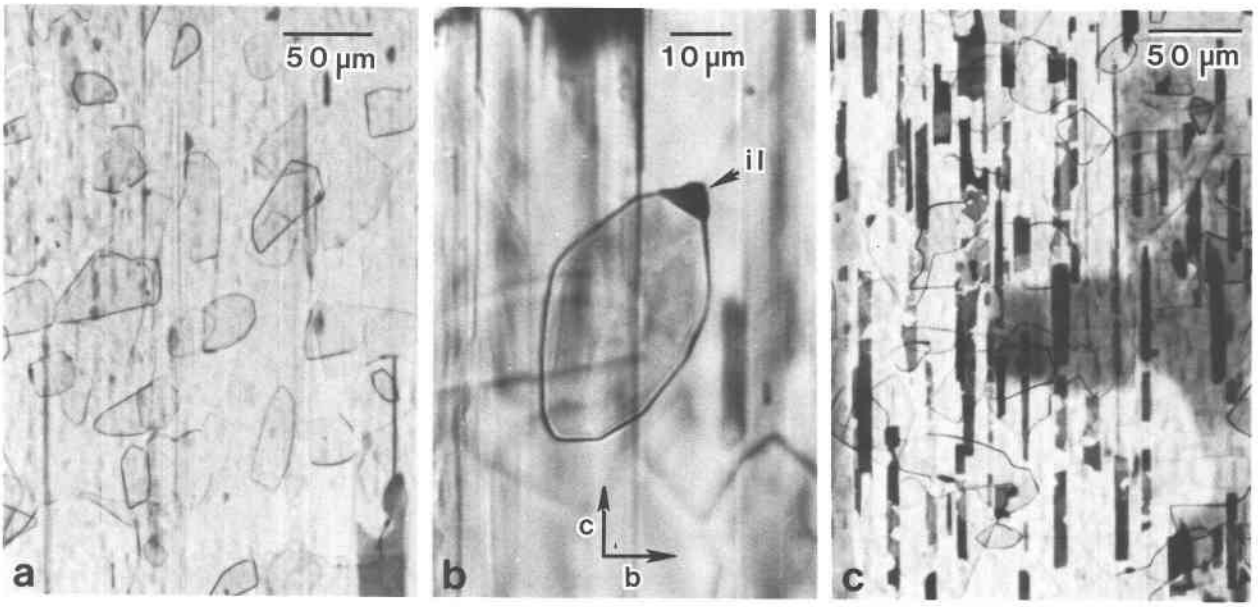

Fig. 11. Oxide lamellae in thin section cut parallel to (100), as seen in plane-polarized light. Crystallographic axes refer to orthopyroxene host. (**a**) Irregularly shaped hercynite lamellae, the outlines of which are marked by dark Becke lines. (**b**) An enlarged view of a hercynite lamella, showing an unusually large marginal crystal of ilmenite (il). (**c**) A group of ilmenite lamellae (dark) elongated parallel to the orthopyroxene *c* axis. Clear hercynite lamellae are also visible in this region.

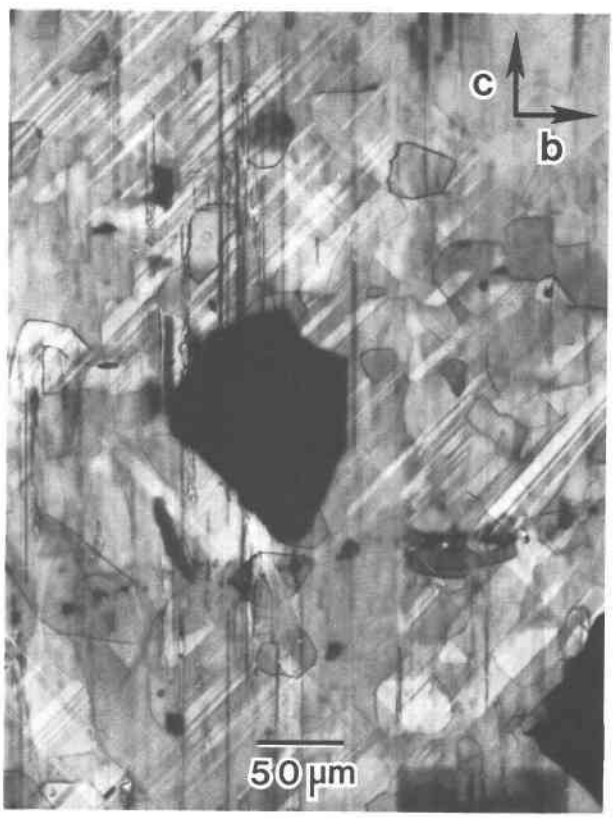

Fig. 12. Cross-hatched twinning in (100) plagioclase lamellae, as seen in cross-polarized light. Crystallographic axes refer to host orthopyroxene. Black lamellae are magnetite, and hercynite is also visible.

millimeters in extent. No features attributable to amphibole were noted in (100) sections.

Plagioclase lamellae

In orthopyroxene (010) and (001) sections, calcic plagioclase can be seen to form lamellae that are typically a few micrometers wide or less. They appear to be relatively straight in (001) sections and less so in (010) sections. The plagioclase lamellae may extend for tens of micrometers up to several millimeters and, as noted above, are commonly interrupted by segments of oxide. The plagioclase is twinned, and the twin planes most typically are inclined to the planes of both (010) and (001) sections. Extinction angle with respect to the *c* axis of the host orthopyroxene is variable but typically larger than that for the amphibole lamellae. In (100) sections, cross-hatched albite and pericline twinning produce a striking and confusing texture in cross-polarized light (Fig. 12). The orientation of the twinning is variable with respect to the host pyroxene axes. However, in most places the traces of the twin planes are inclined to the pyroxene *b* and *c* axes, consistent with the contrast observed in (010) and (001) sections.

In addition to the typical narrow lamellae of plagioclase, a few larger lamellae up to 60 μm thick were observed (Fig. 13a). These larger lamellae are associated with biotite, which presumably forms as a result of unmixing of K from the host pyroxene; such a mechanism was proposed by Morse (1975) to explain the association of potassium feldspar with plagioclase lamellae in a megacryst from the Nain Complex. One large plagioclase

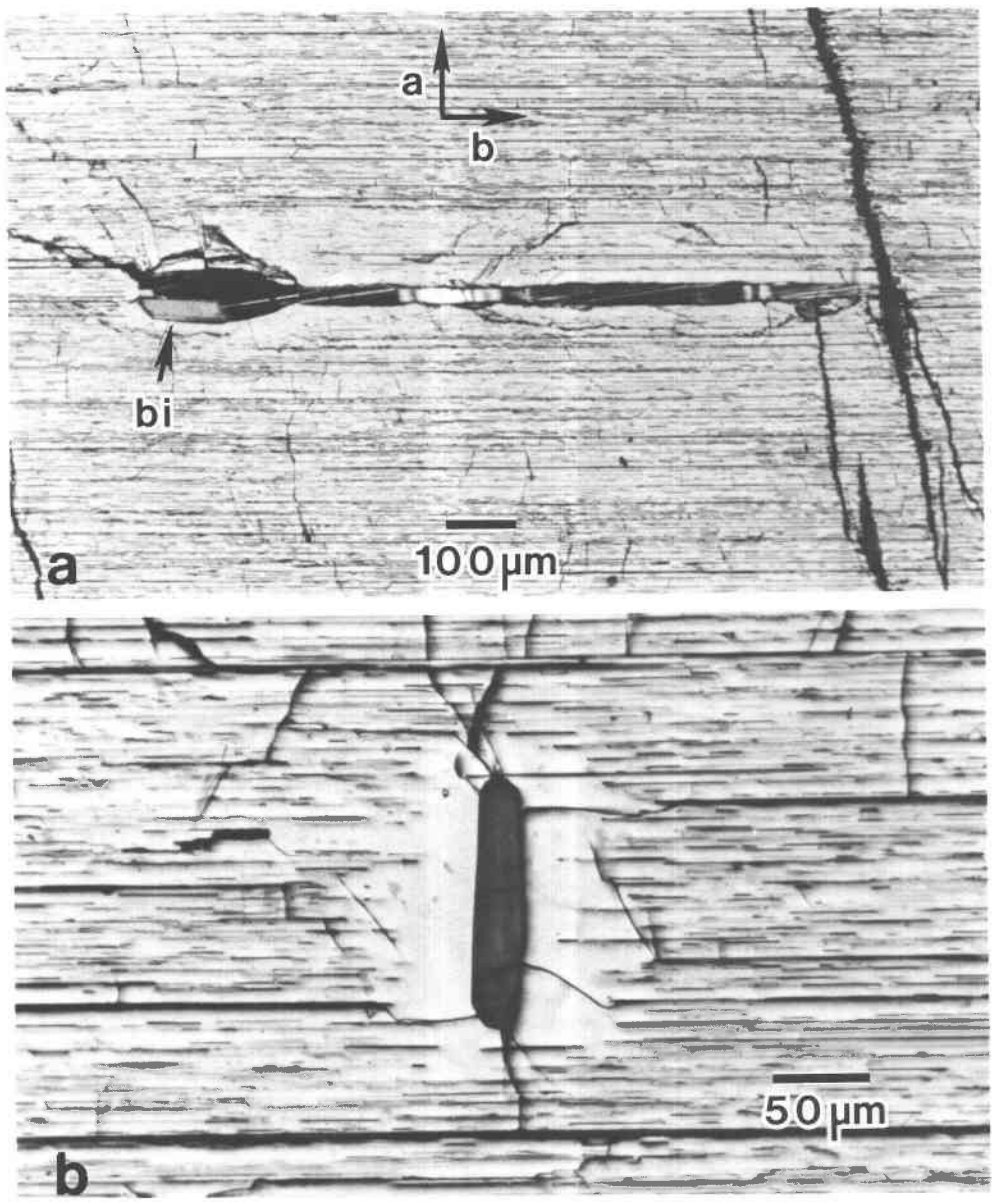

Fig. 13. Large plagioclase lamellae in a (001) thin section, observed in cross-polarized light. (a) Twinned (100) lamella with a marginal biotite crystal (bi). One of the twin orientations is at extinction to show contrast from twinning. (b) A (010) lamella (near extinction) showing obvious precipitate-free zone in surrounding orthopyroxene.

lamella was observed to be oriented parallel to (010), rather than the usual (100) (Fig. 13b). All of the large plagioclase lamellae were observed to be surrounded by precipitate-free zones devoid of narrow lamellae, as shown in Figure 13. Such a texture could result from solute depletion in this zone, if the large lamellae formed early. However, this explanation must be treated with caution, since alteration zones around fractures in this pyroxene also are depleted in or devoid of narrow lamellae, as described below. Thus, precipitate-free zones could result simply from preferential alteration around the large plagioclase lamellae.

Alteration zones associated with fractures

Fractures and associated alteration are obvious in all sections of specimen 1507 that have been examined (Fig. 14). Minerals in these veins or radiating from them that appear to have been produced during alteration include amphibole, chlorite, muscovite, plagioclase, magnetite, and pyrite. The amphibole is oriented with respect to the host pyroxene structure, but the amphibole and other minerals in the alteration zones have a granular habit, rather than the lamellar texture characteristic of the bulk of the specimen. The orthopyroxene in these alteration

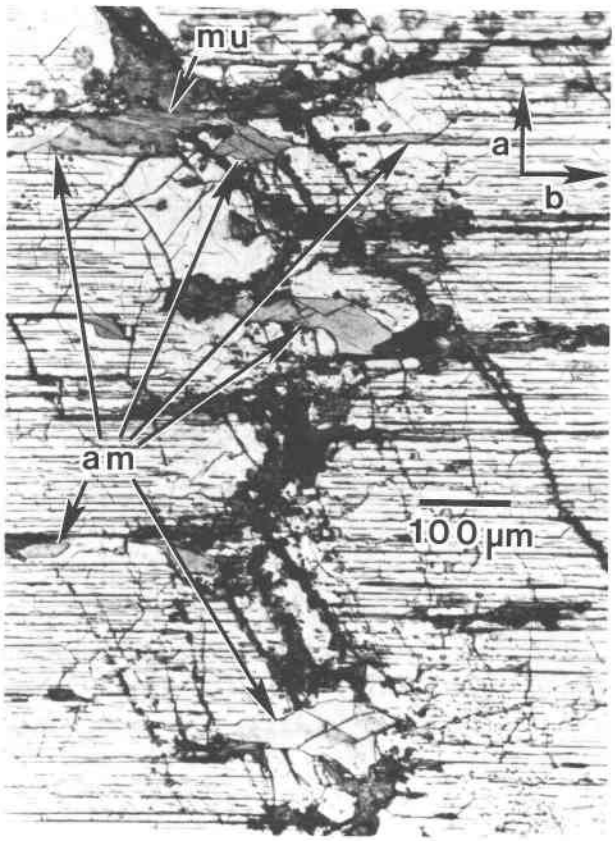

Fig. 14. Alteration zone in (001) section, as seen in plane-polarized light. Dark fractures are filled with fine-grained sheet silicates, and larger crystals of amphibole (am) and muscovite (mu) are indicated. The orthopyroxene surrounding parts of the zone is depleted in (100) lamellae.

zones is generally free from or depleted in (100) lamellae, indicating that the lamellar minerals were dissolved and removed or reprecipitated during the alteration.

Discussion

The textural, crystallographic, and compositional observations on orthopyroxene 1507 confirm that such megacrysts are complex, multiphase intergrowths that can be considered to be pyroxene "rocks" in the parlance of Ross (1970). Likewise, observations on other specimens suggest that (100) lamellae of silicates and oxides may be a common feature of orthopyroxenes having pronounced (100) partings.

The above observations do not appear to place additional constraints on the origin of highly aluminous orthopyroxene megacrysts (i.e., origin by growth at very high pressures versus rapid growth at lower pressures favoring metastably high Al contents). However, the microstructural and compositional characteristics are consistent with subsolidus formation of lamellae in the orthopyroxene, rather than formation by coprecipitation (see Dymek and Gromet, 1984, p. 318, for example).

The TEM-scale observations demonstrate that orthopyroxene 1507 experienced a protracted subsolidus reaction history following initial precipitation of the exsolution lamellae. Compositions of orthopyroxene and clinopyroxene lamellae suggest equilibration to relatively low temperatures on the order of 500–700 °C. In addition, almost total replacement of clinopyroxene lamellae by amphibole, as well as reaction to hydrous mineral assemblages along fractures, suggests that this megacryst experienced extensive hydrothermal alteration following initial precipitation of plagioclase, oxides, and augite. This suggests that hydrothermal alteration may play an important part in the late-stage history of some anorthosites. Since it appears that the alteration did not affect plagioclase lamellae, such pervasive interaction with hydrothermal fluids may have escaped notice previously. Further work on petrologically well-characterized megacrysts is necessary to determine whether such alteration is commonplace in Precambrian anorthosite massifs.

The oxide and silicate lamellae other than plagioclase are rigorously oriented with respect to the host. In all cases, planes of oxygens that are in closest packing or positions near those of closest packing are parallel to orthopyroxene (100). As discussed by numerous authors (e.g., Fleet and Arima, 1985), such topotactic control of intergrowth orientation probably results from the shared structural elements between the lamellae and host. However, the topotactic relationships also produce relatively small misfits in the shared lattice parameters (Table 2), leading to interfaces having low strain. The case of the plagioclase lamellae is interesting in that the plagioclase lattice possesses variable orientations with respect to that of the host. The almost universal interface orientation parallel to the orthopyroxene (100) suggests that the pyroxene structure alone controls interface orientation with feldspar, the pseudo-closest-packed (100) oxygen planes yielding the lowest interface energies regardless of plagioclase orientation.

Acknowledgments

This work was supported by National Science Foundation grants EAR8306861, EAR8609277, and EAR7920095. Electron microscopy was performed at the Johns Hopkins high-resolution TEM laboratory, which was established with partial support from NSF grant EAR8300365. We thank Eric Windsor and Kenneth Livi for helpful discussions, and useful reviews were provided by Ian Mackinnon, Ross Angel, and Richard Reeder.

References cited

Aden, G.D., and Buseck, P.R. (1979) Rapid quantitative analysis of individual particles by energy dispersive spectrometry. In Dale Newberry, Ed., Microbeam analysis, p. 254–258. San Francisco Press, San Francisco.

Bohlen, S.R., and Essene, E.J. (1978) Igneous pyroxenes from metamorphosed anorthosite massifs. Contributions to Mineralogy and Petrology, 65, 433–442.

Buseck, P.R., Nord, G.L., Jr., and Veblen, D.R. (1980) Subsolidus phenomena in pyroxenes. Mineralogical Society of America Reviews in Mineralogy, 7, 117–211.

Cliff, G., and Lorimer, G.L. (1975) The quantitative analysis of thin specimens. Journal of Microscopy, 103, 203–207.

Deer, W.A., Howie, R.A., and Zussman, J. (1978) Rock-forming minerals, vol. 2a, Single-chain silicates. Wiley, New York.

Desnoyers, C. (1975) Exsolutions d'amphibole, de grenat et de spinelle dans les pyroxenes de roches ultrabasiques: Peridotite et pyroxenolites. Bullétin de la Société Français de Minéralogie et Cristallographie, 98, 65–77.

Dymek, R.F., and Gromet, L.P. (1984) Nature and origin of orthopyroxene megacrysts from the St-Urbain anorthosite massif, Quebec. Canadian Mineralogist, 22, 297–326.

Emslie, R.F. (1975) Pyroxene megacrysts from anorthositic rocks: New clues to the sources and evolution of the parent magmas. Canadian Mineralogist, 13, 138–145.

Fleet, M.E., and Arima, M. (1985) Oriented hematite inclusions in sillimanite. American Mineralogist, 70, 1232–1237.

Gilbert, M.C., Helz, R.T., Popp, R.K., and Spear, F.S. (1982) Experimental studies of amphibole stability. Mineralogical Society of America Reviews in Mineralogy, 9B, 229–353.

Iijima, S., and Buseck, P.R. (1975) High resolution electron microscopy of enstatite I: Twinning, polymorphism and polytypism. American Mineralogist, 60, 758–770.

Isaacs, A.M., Brown, P.E., Valley, J.W., Essene, E.J., and Peacor, D.R. (1981) An analytical electron microscopic study of a pyroxene-amphibole intergrowth. Contributions to Mineralogy and Petrology, 77, 115–120.

Leake, B.E. (1978) Nomenclature of amphiboles. American Mineralogist, 63, 1023–1052.

LeFèvre, C. (1969) Remarques sur la valeue du paramétre *b* de la maile des clinopyroxènes. Bullétin de la Société Française Minéralogie et Cristallographie, 92, 95–98.

Lindsley, D.H. (1983) Pyroxene thermometry. American Mineralogist, 68, 477–493.

Livi, K.J.T., and Veblen, D.R. (1987) "Eastonite" from Easton, Pennsylvania: A mixture of phlogopite and a new form of serpentine. American Mineralogist, 72, 113–125.

Mellini, M., Oberti, R., and Rossi, G. (1983) Crystal-chemistry and microstructures of pyroxenes and amphiboles in the coronas of the Bergen arcs and of the Sognefjord region, western Norway. Periodico di Mineralogia—Roma, 52, 583–615.

Morse, S.A. (1975) Plagioclase lamellae in hypersthene, Tikkoatokhakh Bay, Labrador. Earth and Planetary Science Letters, 26, 331–336.

——— (1979) Kiglapait geochemistry. I. Systematics, sampling, and density. Journal of Petrology, 20, 555–590.

Myklebust, R.L., Fiori, C.E., and Heinrich, K.F.J. (1978) FRAMEC: A compact procedure for quantitative energy-dispersive electron probe X-ray analysis. U.S. National Bureau of Standards Technical Memorandum.

Nakajima, Y., and Ribbe, P.H. (1980) Alteration of pyroxenes from Hokkaido, Japan, to amphibole, clays, and other biopyriboles. Neues Jahrbuch für Mineralogie Monatshefte, 258–268.

Ross, M. (1970) Chemical reactions in pyroxene crystals. American Mineralogist, 55, 310–311.

Smith, P.P.K. (1977) An electron microscope study of amphibole lamellae in augite. Contributions to Mineralogy and Petrology, 59, 317–322.

Veblen, D.R. (1985) Direct TEM imaging of complex structures and defects in silicates. Annual Review of Earth and Planetary Sciences, 13, 119–146.

——— (1981) Non-classical pyriboles and polysomatic reactions in biopyriboles. Mineralogical Society of America Reviews in Mineralogy, 9A, 189–236.

Veblen, D.R., and Buseck, P.R. (1981) Hydrous pyriboles and sheet silicates in pyroxenes and uralites: Intergrowth microstructures and reaction mechanisms. American Mineralogist, 66, 1107–1134.

Yamaguchi, Y., Arai, J., and Tomita, K. (1978) Clinoamphibole lamellae in diopside of garnet lherzolite from Alpe Arami, Bellinzona, Switzerland. Contributions to Mineralogy and Petrology, 66, 263–270.

MANUSCRIPT RECEIVED JUNE 8, 1987
MANUSCRIPT ACCEPTED MARCH 15, 1988